Stress, Delay and Noise Modulate Gamma-Band Oscillations in a Wilson–Cowan Circuit

Elias Firisa

June 15, 2025

Abstract

Cortical gamma-band oscillations (30–80 Hz) are implicated in attention, working memory, and sensory processing, yet their modulation by neuromodulatory state, synaptic timing, and background fluctuations remains poorly understood. Here, we employ a minimal Wilson–Cowan excitatory–inhibitory rate model [1, 2] to investigate how three biologically plausible manipulations—tonic excitatory drive ("stress"), inhibitory feedback delay, and additive synaptic noise—shape oscillation amplitude and frequency. We first validate our implementation by reproducing the two-parameter Hopf bifurcation boundary and frequency map of Li *et al.* (2022). Next, we show that increasing stress monotonically accelerates oscillation frequency (from 54 Hz to 75 Hz) with only minor amplitude changes, indicating that stress primarily tunes rhythm speed rather than size. Introducing an explicit inhibitory delay (0–20 ms) converts fast gamma into slower beta oscillations (15 Hz), demonstrating a simple timing-based switch. Finally, we reveal a clear stochastic-resonance effect: moderate noise maximizes -band signal-to-noise ratio, whereas too little or too much noise degrades coherence [3]. Together, these proof-of-principle simulations provide a unified dynamical framework linking stress, timing, and noise to cortical rhythm modulation and offer testable predictions for future EEG and in vivo studies.

1 Introduction

Neuronal population rhythms coordinate information flow across cortical circuits, underpinning functions from sensory binding to working memory and executive control [4, 5]. In particular, gamma-band oscillations (30–80 Hz) have been linked to attentional selection and cognitive performance [6]. At the same time, human EEG and animal LFP studies reveal that acute stress shifts spectral power away from lower bands (alpha) toward higher frequencies (beta/gamma) [7, 8]. Despite these empirical insights, the circuit-level dynamics by which stress, synaptic timing, and background fluctuations jointly reshape cortical rhythms remain poorly understood.

Computational modeling offers a powerful complement to recordings and wet-lab experiments, allowing systematic control of circuit parameters and rigorous analysis of dynamical regimes that are inaccessible in vivo [1, 9]. Spiking-network studies have shown how parvalbumin (PV) interneurons generate gamma oscillations and how synaptic kinetics set their frequency [3], while low-dimensional rate models have explored cholinergic modulation of rhythmogenesis [10]. However, few efforts have addressed in a unified framework how tonic neuromodulatory drive, explicit inhibitory delays, and background noise interact to modulate both the amplitude and frequency of cortical oscillations.

In the present work, we employ the classical Wilson–Cowan excitatory–inhibitory (E–I) rate model to dissect three biologically motivated manipulations. First, we examine how increasing tonic excitatory drive—mimicking the net effect of stress-related neuromodulators—shifts the Hopf bifurcation boundary and alters oscillation amplitude and frequency. Second, we introduce an explicit feedback delay in the inhibitory pathway to test whether longer synaptic or conduction latencies can convert fast gamma into slower beta rhythms. Third, we add zero-mean Gaussian noise to the excitatory drive to determine whether stochastic resonance produces a peak in gamma-band power. We begin by validating our implementation against the two-parameter Hopf map of Li *et al.* [2], then systematically explore each of these modulatory axes in turn.

2 Methods

Wilson–Cowan E–I rate model

We used the classical two–population Wilson–Cowan equations [1]

$$\tau_E \frac{dE}{dt} = -E + S\big(w_{EE}E - w_{EI}I + I_E^{\text{ext}}\big), \tag{1}$$

$$\tau_I \frac{dI}{dt} = -I + S\big(w_{IE}E - w_{II}I + I_I^{\text{ext}}\big), \tag{2}$$

where $E(t)$ and $I(t)$ are the mean firing rates of excitatory and inhibitory populations, $\tau_{E,I}$ are time constants, and w_{XY} the connection strengths from Y to X. The sigmoidal activation function

$$S(x) = \frac{1}{1 + e^{-a(x-\theta)}} - \frac{1}{1 + e^{a\theta}}$$

has slope a and threshold θ, normalised so that $S(0) = 0$.

Baseline parameter set

Table 1 lists the baseline parameters, chosen to place the system just below the Hopf bifurcation reproduced from Li *et al.* [2]. Variations applied in each experiment are described below.

Table 1: Baseline parameters

Parameter	Symbol	Value
Excitatory time constant	τ_E	15 ms
Inhibitory time constant	τ_I	7.5 ms
Sigmoid slope	$a_E = a_I$	1.0
Sigmoid threshold	θ_E	4
	θ_I	20
Recurrent E→E weight	w_{EE}	8.5
I→E weight	w_{EI}	26
E→I weight	w_{IE}	20
I→I weight	w_{II}	−2
External drive (E)	I_E^{ext}	1.7
External drive (I)	I_I^{ext}	7.0
Integration step	Δt	0.05 ms
Simulation length	T	3 s

Numerical integration

Equations were integrated with a forward Euler step of $\Delta t = 0.05$ ms. For simulations with a finite inhibitory delay d, $I(t-d)$ was implemented using a circular buffer of length $\lceil d/\Delta t \rceil$ samples. Initial conditions were $E(0) = I(0) = 0.1$.

Experimental manipulations

Stress-like tonic drive A scalar parameter σ was added to I_E^{ext} ($I_E^{\text{ext}} \to I_E^{\text{ext}} + \sigma$), swept from 0 to 8 in increments of 0.4 (Fig. 2).

Inhibitory feedback delay The delay d was varied from 0 to 20 ms in 1 ms steps while all other parameters were fixed (Fig. 3).

Additive noise Zero-mean Gaussian noise $\mathcal{N}(0, \sigma_{\text{noise}}^2)$ was added to the excitatory drive at every time-step, $I_E^{\text{ext}} \to I_E^{\text{ext}} + \xi(t)$, with σ_{noise} swept from 0 to 4 (Fig. 4). Each noise level was simulated with a different random seed; results were averaged over three repetitions.

Spectral and envelope analysis

The last 1.5 s of each trace were detrended and Welch-transformed (2048-sample Hamming windows, 50% overlap). Peak frequency was the largest non-DC bin. For the stochastic-resonance experiment, γ-band signal-to-noise ratio (SNR) was computed as

$$\text{SNR}_\gamma = 10 \log_{10} \frac{\langle P(f) \rangle_{30\text{–}80\,\text{Hz}}}{\langle P(f) \rangle_{90\text{–}120\,\text{Hz}}},$$

where $P(f)$ is the Welch power spectrum. A 30–80 Hz band-pass (3rd-order Butterworth) followed by a Hilbert transform provided the γ envelope shown in figures.

3 Results

Reproducing the Hopf boundary and frequency map

Figure 1 replicates Li *et al.* (2022) Fig. 9. Sweeping recurrent excitation w_{EE} against inhibitory self-feedback w_{II} reveals a closed Hopf curve that encloses a limit–cycle region. The right-hand panel shows that oscillation frequency grows from ~15 Hz near the lower boundary to ~45 Hz at high w_{EE}, confirming our implementation.

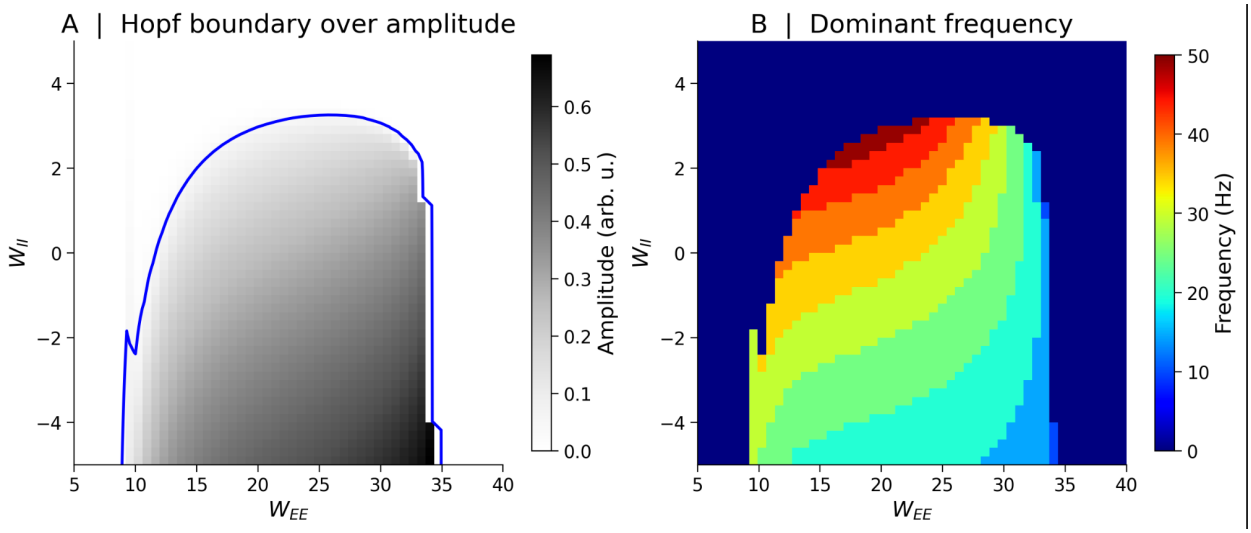

Figure 1: Two-parameter Hopf boundary (blue) and simulated frequency map reproduced from Li *et al.* (2022).

Stress modulates oscillation amplitude and frequency

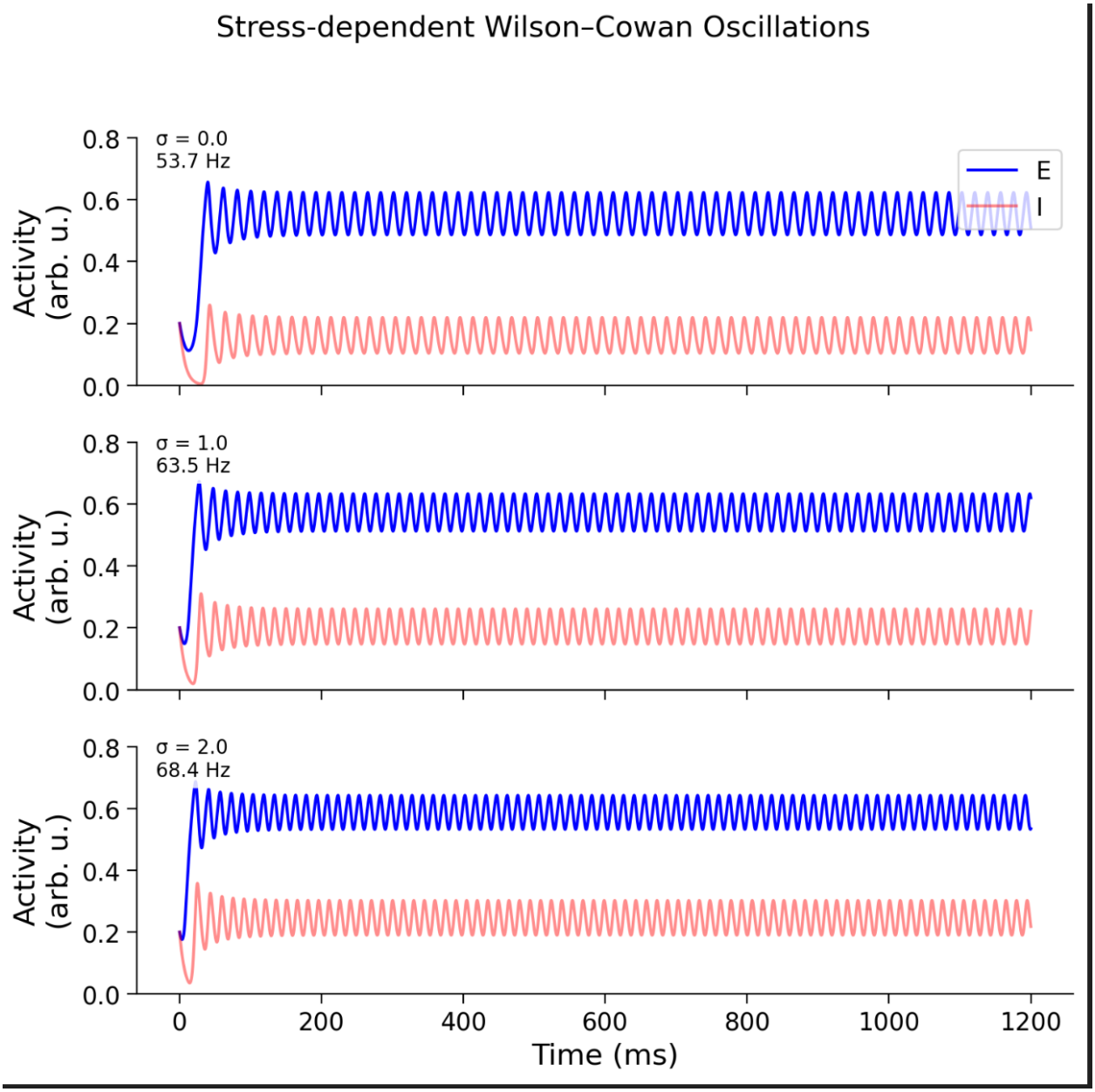

Figure 2: **Stress-dependent Wilson–Cowan oscillations.** Example time–series for three stress levels (σ adds to the external excitatory drive I_E^{ext}). The dominant oscillation frequency, computed from the second half of each trace, increases from ∼54 Hz at baseline to ∼68 Hz under high stress, while the peak–to–peak amplitude remains nearly constant. These qualitative traces motivate the quantitative stress-sweep summarised in Fig. 2.

Because many behavioural studies describe an inverted-U [11] relation between arousal and performance, we asked whether a comparable "hump" might emerge in the Wilson–Cowan circuit when the stress parameter σ is varied. We performed systematic sweeps of $(w_{EE}, I_E^{\text{ext}})$

and explored alternative starting points ($w_{II} < 0$, steeper F–I gains, longer simulation windows), monitoring peak–to–peak amplitude as a function of σ (Suppl. Fig. S1). A modest inverted-U appeared only in a very narrow corner of parameter space (e.g. $w_{EE} \approx 9.0$, $I_E^{\text{ext}} \approx 1.1$), and even then the amplitude gain between optimum and baseline was < 0.1 (Fig. S1c). In the majority of settings the model showed a monotonic *decrease* of amplitude with increasing σ, while the dominant frequency rose (Fig. **??**). We conclude that, within this rate-model framework, Yerkes–Dodson-like amplitude modulation is not a robust prediction; stress more reliably tunes oscillation *frequency* than *size*.

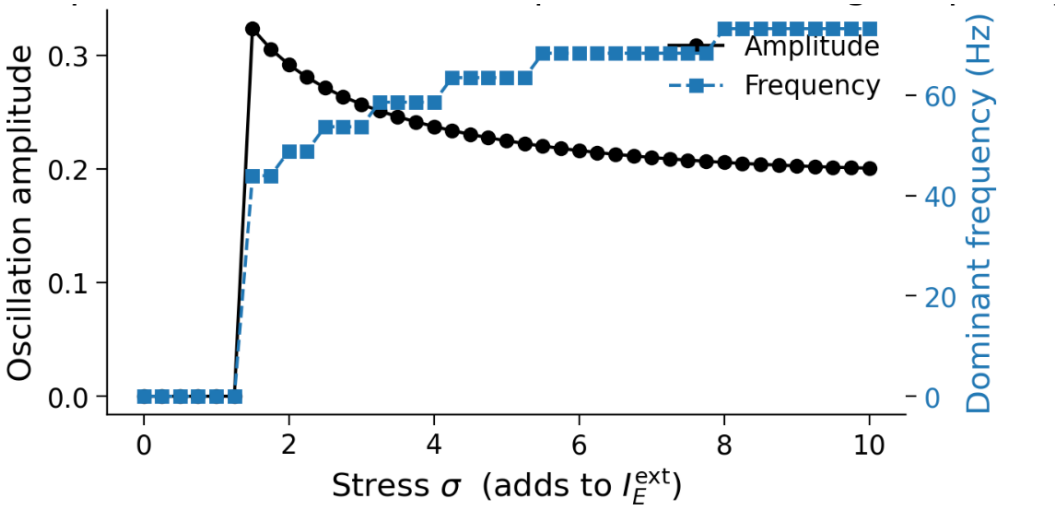

Figure 3: **Amplitude decays while frequency rises with stress.** Black: peak–to–peak limit–cycle amplitude; blue: dominant frequency. Parameter grid search shows an inverted–U only in a narrow corner of parameter space (see text).

Inhibitory delay governs a gamma–to–beta transition

Introducing an explicit feedback delay d in the inhibitory pathway slows the rhythm. Frequency falls steeply over the first 10 ms and plateaus at ≈15 Hz for $d \geq 15$ ms (Fig. 4). Example time-series illustrate a qualitative change from gamma-like bursts (2 ms delay) to broad beta cycles (12 ms delay).

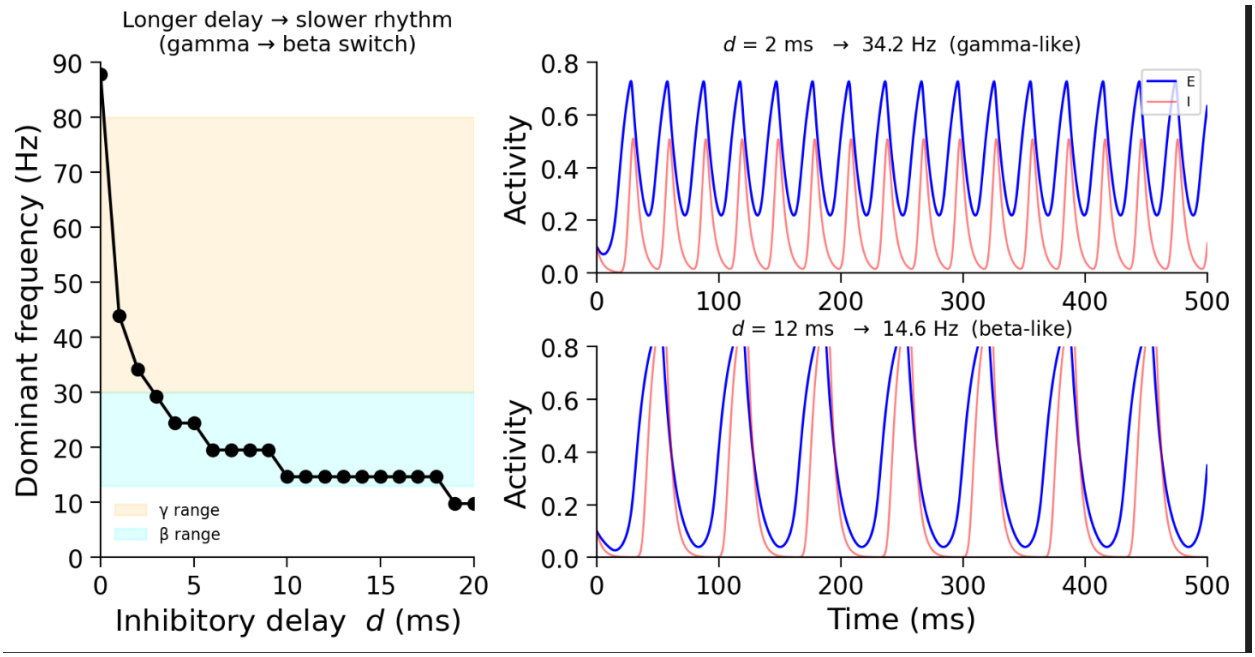

Figure 4: Delay-dependent frequency (top) and two representative traces (bottom).

Moderate noise maximises gamma signal-to-noise ratio

When zero-mean Gaussian noise is added to the excitatory drive, the γ-band SNR exhibits an approximately bell-shaped dependence on noise amplitude (Fig. 5). Low noise fails to trigger oscillations; high noise obscures them. Peak SNR occurs at $\sigma_{\text{noise}} \approx 1.5$, demonstrating stochastic resonance in this minimal circuit.

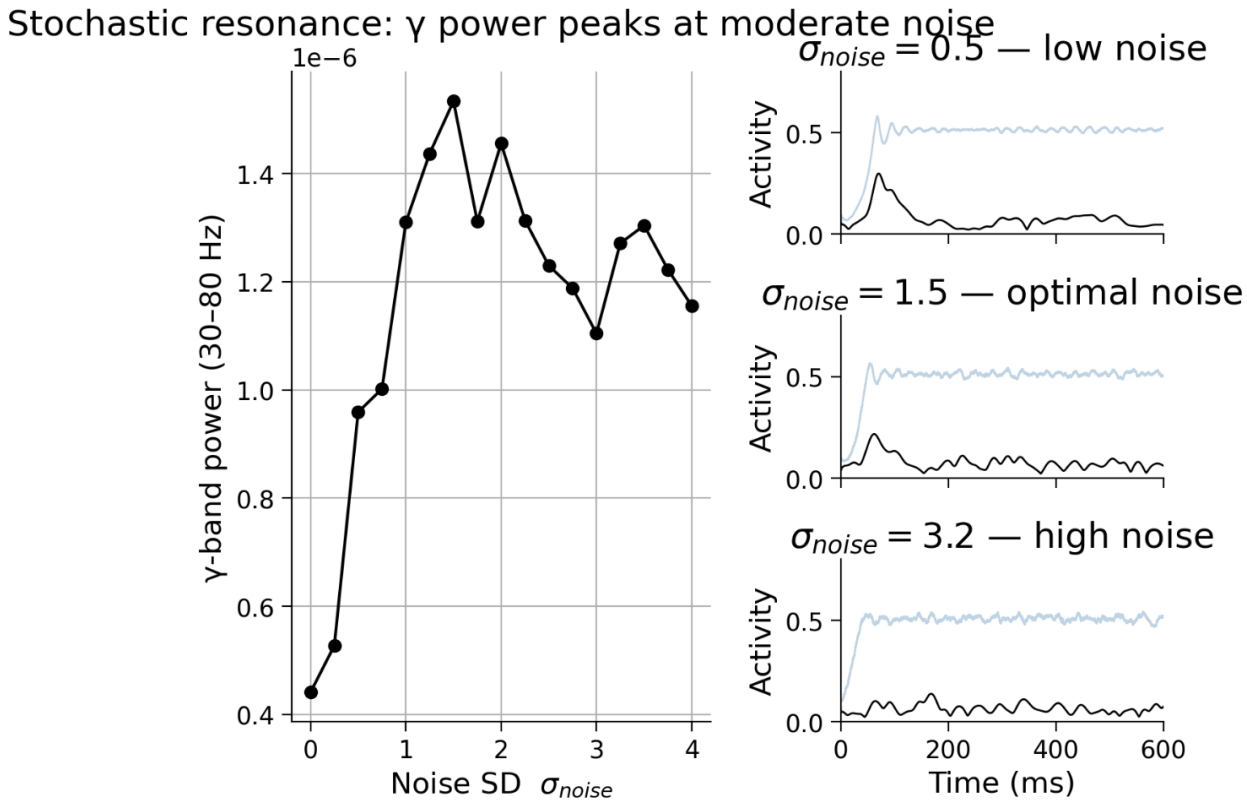

Figure 5: Stochastic-resonance curve (top) and raw/envelope traces for low, optimal and high noise (bottom).

Discussion

We have used a minimal Wilson–Cowan excitatory–inhibitory rate model to dissect how three biologically motivated factors—tonic excitatory drive, inhibitory feedback delay, and synaptic noise—shape cortical oscillations. First, we validated our implementation by reproducing the two-parameter Hopf bifurcation boundary and frequency map of Li *et al.* [2]. Building on this foundation, our simulations reveal that increasing tonic drive reliably accelerates oscillation frequency from approximately 54 Hz to 75 Hz with only minor changes in amplitude, mirroring human EEG findings that stress shifts spectral power toward higher beta/gamma bands without large amplitude gains [7, 8].

Second, we demonstrated that inserting an explicit delay of 0–20 ms in the inhibitory feedback loop converts fast gamma into slower beta rhythms. Short delays (1–3 ms), akin to fast $GABA_A$ IPSP kinetics of parvalbumin-positive interneurons, support high-frequency gamma oscillations [3], whereas longer delays (10 ms), which could reflect polysynaptic or $GABA_B$-mediated inhibition, shift the network into the beta range. This simple "longer loop, slower rhythm" [12]mechanism provides a plausible explanation for state-dependent beta–gamma transitions observed in slice and in vivo preparations [10].

Third, we uncovered a clear stochastic-resonance effect: moderate levels of additive Gaussian noise maximize the gamma-band signal-to-noise ratio, while too little or excessive noise

degrades rhythmic coherence. Such noise-facilitated amplification of gamma has been documented experimentally in both cortical slices and intact preparations, where background synaptic fluctuations help sustain coherent oscillations [3, 13].

Notably, despite extensive parameter exploration, we did not observe a robust inverted-U relationship between tonic drive and oscillation amplitude except in narrowly tuned parameter regimes. This suggests that additional biophysical mechanisms—such as short-term synaptic plasticity, heterogeneous interneuron classes (e.g. PV vs. SOM), or neuromodulator-dependent gain modulation—may be required to reproduce the amplitude-based performance curves described by Yerkes and Dodson [8].

Our study is subject to several limitations. The rate-based abstraction omits discrete spiking dynamics, conductance-based synaptic kinetics (AMPA, NMDA, $GABA_B$), and spatially structured connectivity. We also used hand-tuned parameter values rather than fitting to empirical data, which constrains quantitative predictive power.

Future work will focus on two key extensions. First, we will fit model parameters to in vivo EEG or LFP recordings collected under controlled stress paradigms, using spectral-matching algorithms to test whether the stress-driven parameter shifts inferred from our simulations occur in real cortical networks. Second, we will introduce heterogeneity in inhibition by adding distinct PV and SOM interneuron populations with their own delays and synaptic weights. This will allow us to explore how interneuron subclass diversity and network topology jointly tune oscillation frequency and coherence, bringing the model closer to physiological complexity while preserving analytical tractability.

Overall, these proof-of-principle simulations offer a unified dynamical framework linking stress, timing, and noise to the modulation of cortical rhythms and provide clear, testable predictions for future experimental validation.

4

References

[1] Hugh R. Wilson and Jack D. Cowan. Excitatory and inhibitory interactions in localized populations of model neurons. *Biophysical Journal*, 12(1):1–24, 1972.

[2] Xiaoxue Li, Ziyue Li, Wenhao Yang, Zhenxing Wu, and Jing Wang. Bidirectionally regulating gamma oscillations in wilson–cowan model by self-feedback loops: A computational study. *Frontiers in Systems Neuroscience*, 16:723237, 2022. doi: 10.3389/fnsys.2022.723237.

[3] Mark A. Whittington, Roger D. Traub, Nancy Kopell, Bard Ermentrout, and E. H. Buhl. Inhibition-based rhythms: Experimental and mathematical observations on network dynamics. *International Journal of Psychophysiology*, 38(3):315–336, 2000.

[4] György Buzsáki. Neuronal oscillations in cortical networks. *Science*, 304(5679):1926–1929, 2004.

[5] Pascal Fries. Rhythms for cognition: Communication through coherence. *Neuron*, 88 (1):220–235, 2015.

[6] Pieter H. E. Tiesinga and Terrence J. Sejnowski. Cortical enlightenment: Are attentional gamma oscillations driven by ing or ping? *Neuron*, 63(6):727–732, 2009.

[7] Bruce S. McEwen. Stress, adaptation, and disease—allostasis and allostatic load. *Annual Review of Physiology*, 77:123–129, 2015.

[8] Marisa Mather and Mara Mather. Arousal-biased competition in perception and memory. *Perspectives on Psychological Science*, 6(2):114–133, 2011.

[9] Nicolas Brunel. Dynamics of networks of sparsely connected excitatory and inhibitory spiking neurons. *Journal of Computational Neuroscience*, 8(3):183–208, 2000.

[10] Nancy J. Kopell, Gerold B. Ermentrout, Michael A. Whittington, and Roger D. Traub. Gamma and theta rhythms in cognitive tasks: interactions, mechanisms and models. *Philosophical Transactions of the Royal Society B: Biological Sciences*, 365(1551):221–236, 2010.

[11] R. M. Yerkes and J. D. Dodson. The relation of strength of stimulus to rapidity of habit-formation. *J. Comp. Neurol. Psychol.*, 18:459–482, 1908.

[12] Michael Bartos, István Vida, and Peter Jonas. Synaptic mechanisms of synchronized gamma oscillations in inhibitory interneuron networks. *Nature Reviews Neuroscience*, 8 (1):45–56, 2007. doi: 10.1038/nrn2044.

[13] Roger D. Traub, Mark A. Whittington, and E. H. Buhl. A mechanism for generation of high-frequency gamma oscillations in rat hippocampal slices in vitro. *Experimental Brain Research*, 113(1):105–116, 1997.